Evolutionary dynamics on rugged fitness landscapes: Exact dynamics and information theoretical aspects

David B. Saakian[1,2] and José F. Fontanari[1]
[1]*Instituto de Física de São Carlos, Universidade de São Paulo, Caixa Postal 369, 13560-970 São Carlos, SP, Brazil*
[2]*Yerevan Physics Institute, Alikhanian Brothers Street 2, Yerevan 375036, Armenia*
(Received 7 May 2009; published 2 October 2009)

The parallel mutation-selection evolutionary dynamics, in which mutation and replication are independent events, is solved exactly in the case that the Malthusian fitnesses associated to the genomes are described by the random energy model (REM) and by a ferromagnetic version of the REM. The solution method uses the mapping of the evolutionary dynamics into a quantum Ising chain in a transverse field and the Suzuki-Trotter formalism to calculate the transition probabilities between configurations at different times. We find that in the case of the REM landscape the dynamics can exhibit three distinct regimes: pure diffusion or stasis for short times, depending on the fitness of the initial configuration, and a spin-glass regime for large times. The dynamic transition between these dynamical regimes is marked by discontinuities in the mean-fitness as well as in the overlap with the initial reference sequence. The relaxation to equilibrium is described by an inverse time decay. In the ferromagnetic REM, we find in addition to these three regimes, a ferromagnetic regime where the overlap and the mean-fitness are frozen. In this case, the system relaxes to equilibrium in a finite time. The relevance of our results to information processing aspects of evolution is discussed.

DOI: 10.1103/PhysRevE.80.041903 PACS number(s): 87.10.−e, 87.15.A−, 87.23.Kg, 02.50.−r

I. INTRODUCTION

Evolution on complex fitness landscapes has been advanced as a key idea in recent mathematical approaches to evolution theory [1,2]. Concepts such as neutral networks and punctuated equilibrium, which are central to such disparate areas as molecular evolution and paleontology, can be brought together within that unifying framework. Since frustration and quenched disorder combined together yield an almost infallible recipe to generate complexity [3], the evolutionary dynamics on rugged fitness landscapes became a research topic in the statistical mechanics of disordered systems.

There are a few reasons to consider spin-glass or random fitness landscapes in the study of molecular evolution. Fitness functions are related to the binding affinity of a molecular replicator (a RNA-like molecule) to a nonspecific replicase [4]. Given our present incapacity to predict affinity—single amino acid replacements may prevent binding altogether, increase affinity by orders of magnitude, or simply leave it unaffected [5]—the assignment of fitness values chosen at random from some probability distribution seems to be the least biased course to introduce fitness in evolution models. In addition, evolution in any fitness landscape characterized by a finite correlation length will resemble evolution in a random landscape when viewed at an appropriate coarse-grained scale of the sequence configuration space [6]. Finally, the analysis of the evolution on rugged or random fitness landscapes has produced dynamical patterns, such as punctuated equilibria (see [7,8]), that are actually observed in microbial populations [9].

Building on a mapping between the infinite-population quasispecies model [10] and an anisotropic two-dimensional Ising spin model in which the time t is one of the lattice dimensions [11,12], the evolutionary version of Derrida's random energy model (REM) [13,14] was solved exactly in the infinite-time, equilibrium regime [15,16]. Two distinct phases were found, corresponding to the selective and nonselective regimes that characterize a model that exhibits an error threshold transition (see also [17]). More recently, the dynamics of this model was investigated in the limit of strong selection using approximate techniques [18–21]. Since strong selection is not the only biologically relevant situation, and the selective regime is not the only important dynamic regime, a more general approach to the dynamics of the evolutionary version of REM is necessary.

In this contribution, we explore a different mapping between evolutionary dynamics and statistical physics, namely, the mapping between the parallel mutation-selection scheme and the quantum Ising chain in a transverse field [22], to solve exactly the dynamics on REM-like fitness landscape for all range of the selection and mutation parameters. This approach was already successfully used in the analysis of a simpler fitness landscape, the Single-Peak fitness landscape [23] and is based on the results of Refs. [24,25]. A more recent application was the solution of the evolutionary dynamics in the case of symmetric fitness landscapes (i.e., the fitness is a function of the Hamming distance from a given reference sequence) [26].

Here we consider two landscapes, the ordinary REM landscape and the ferromagnetic REM landscape, where one of the energy levels of the ordinary REM is selected and changed to an energy value lower than the typical ground-state energy. For both landscapes, we find that the dynamic behavior for short times depends on the (Malthusian) fitness of the initial configuration. When the fitness of the initial configuration is higher than the mutation rate, the dynamics freezes at the initial configuration, resulting in a pattern of stasis (provided that the initial fitness is not the global maximum). Otherwise, when the initial fitness is lower than the mutation rate, the dynamics is characterized by a regime of pure diffusion in the sequence space. In the ordinary REM,

we find that these short-time regimes—diffusion or stasis—change abruptly to a spin-glass-like regime, which is associated to the equilibrium frozen phase of the REM. This dynamic transition is signaled by a discontinuity of the mean fitness as well as of the average overlap with the initial, reference sequence. Most importantly, we find that these quantities tend to their equilibrium values as $1/t$ for large time t. In the case of the ferromagnetic REM we find up to four distinct dynamic regimes: diffusion or stasis, spin glass and ferromagnetic. As before, the transitions between these regimes are signaled by discontinuities in the biologically relevant observables, but the system relaxes to the equilibrium ferromagnetic state in a finite time.

Our results are interesting for the statistical physics aspects of information theory as well [27–32], as REM statistical physics gives a simple derivation of most of information theory results. The idea of coding via statistical mechanics is to construct a spin Hamiltonian, which has a known ground state for a specific choice of the deterministic spin couplings (the nontrivial aspect of the problem is that the ground state of the Hamiltonian should be robust to some degree of noise in those couplings). The ground state of the Hamiltonian could then be recovered from the starting configuration using some update dynamics, as in the case of associative memory neural networks [33]. Thus, by solving an evolution model we get as a by-product an analytical decoding dynamics for optimal codes.

The rest of the paper is organized as follows. In Sec. II we introduce the evolution equations for the parallel mutation-selection scheme and discuss its relation with the quantum Ising chain in a transverse field. The basic equations for the dynamics obtained using the Suzuki-Trotter formalism [34] are introduced also in that section. In Sec. III we review the main results obtained in the analysis of the single-peak landscape [23] as they underlie most of the arguments used in the solution of the more complex landscapes. In Secs. IV and V we present the exact solution of the evolutionary dynamics of the ordinary REM and of ferromagnetic REM, respectively. Finally, in Sec. VI we summarize our main results and present some concluding remarks.

II. ISING QUANTUM CHAIN FORMULATION

In this contribution, we consider the so-called parallel mutation-selection scheme in which mutation and selection are considered as independent events [35–37], i.e., mutations can occur at any time during the existence of a sequence, not only at the moment of replication as assumed in Eigen's molecular quasispecies model [10]. As usual, we represent a molecule or genome of length N by a sequence of binary digits (spins) $s_k=\pm 1$ with $k=1,\ldots,N$ so that there are 2^N distinct molecules $S^i\equiv(s_1^i,\ldots,s_N^i)$. In the parallel mutation-selection scheme, the relative frequencies of molecules $i=1,\ldots,2^N$ are given by [35]

$$\frac{dp_i}{dt}=p_i\left(r_i-\sum_{j=1}^{2^N}r_jp_j\right)+\sum_{j=1}^{2^N}m_{ij}p_j, \tag{1}$$

where r_i are Malthusian fitnesses, which can take on positive as well as negative values [36], and m_{ij} is the mutation rate from S^i to S^j. Since mutations can connect only nearest neighboring sequences in the 2^N-dimensional sequence space, we choose $m_{ij}=\gamma$ if $d(S^i,S^j)=1$; $m_{ii}=-N\gamma$ and $m_{ij}=0$, otherwise. Here, $d(S^i,S^j)$ is the Hamming distance between sequences S^i and S^j and γ is the mutation rate per site. As $\Sigma_i m_{ij}=0$, the dynamics [Eq. (1)] maintains the normalization $\Sigma_i p_i=1$ for all t. Finally, we recall that $r_i=f(s_1^i,\ldots,s_N^i)$ determines the so-called fitness landscape.

A key observation at this stage is the finding that the nonlinear dynamic system Eq. (1) can be reduced to a linear system

$$\frac{dx_i}{dt}=\sum_j H_{ij}x_j, \tag{2}$$

where $H_{ij}=H_{ji}\equiv r_i\delta_{ij}+m_{ij}$ using the transformation [38]

$$x_i(t)=p_i(t)\exp\left[\sum_j r_j\int_0^t d\tau p_j(\tau)\right]. \tag{3}$$

In practice, we solve the linear system Eq. (2) and then obtain the original sequence frequencies via the normalization $p_i=x_i/\Sigma_j x_j$. From the numerical perspective, solution of this linear system is straightforward, the sole limitation being the exponential increase in the number of equations with the sequence length N.

For certain fitness landscapes, however, the case of infinite length sequences can be solved analytically thanks to a cunning observation by Baake *et al.* [22], who realized that the linear system Eq. (2) can be mapped into an Ising quantum chain in a transverse magnetic field with spin interactions that depend on the specific choice of the fitness landscape. More pointedly, the linear system Eq. (2) is equivalent to the evolution of the quantum system described by the Hamiltonian [22]

$$-\mathcal{H}=\gamma\left(\sum_{k=1}^{N}\sigma_k^x-N\right)+f(\sigma_1^z,\ldots,\sigma_N^z), \tag{4}$$

where $\sigma_k^{x,z}$ stands for the Pauli spin operators acting in site k, i.e., $\sigma_k^{x,z}=1\otimes\ldots 1\otimes\sigma^{x,z}\otimes 1\ldots\otimes 1$ with $\sigma^{x,z}$ in the kth place.

Introducing the time evolution operator $\mathcal{T}(t)=\exp(-\mathcal{H}t)$ we can write a formal expression for the original molecules frequencies, namely,

$$p_j(t)=\frac{1}{\mathcal{N}}\sum_{i=1}^{2^N}Z_{ji}(t)p_i(0), \tag{5}$$

where $Z_{ji}(t)=\langle S^j|\mathcal{T}(t)|S^i\rangle$ and $\mathcal{N}=\Sigma_{ji}Z_{ji}(t)p_i(0)$ guarantees the correct normalization. Here $|S^i\rangle=|\chi_1^i\rangle\otimes\ldots\otimes|\chi_N^i\rangle$ where $|\chi_k^i\rangle$ is an eigenstate of σ_k^z.

Since there is an equivalence between the quantum Ising chain, such as that described by Hamiltonian Eq. (4), and a classical anisotropic two-dimensional Ising spin model [34], then Baake *et al.*'s observation shows that there is a mapping between the parallel mutation-selection evolution scheme and the two-dimensional Ising model. It is interesting that a similar result holds for Eigen's quasispecies model as well [11,12].

The challenge here is to calculate $Z_{ji}(t)$, which is proportional to the probability that state $|S^i\rangle$ transitions to state $|S^j\rangle$ in a time interval of length t. Henceforth, we will refer to Z_{ji} as the transition amplitude between those states. In the case that the spins interaction, i.e., the term $f(\sigma_1^z,\ldots,\sigma_N^z)$ in Eq. (4), can be neglected we have $\mathcal{T}\to\mathcal{T}_{diff}=\exp[\gamma\Sigma_i(\sigma_i^x-1)]$ so that Z_{ji} can be readily evaluated [34] (see also [23]),

$$\langle S^j|\mathcal{T}_{diff}(t)|S^i\rangle = \exp\{N[\phi(m,t)-\gamma t]\}, \tag{6}$$

where

$$\phi(m,t) = \frac{1+m}{2}\ln\cosh(\gamma t) + \frac{1-m}{2}\ln\sinh(\gamma t) \tag{7}$$

and m is the overlap between configurations S^i and S^j, i.e., $m=\Sigma_k s_k^i s_k^j/N$. On the other hand, in the case the interactions are dominant we have $\mathcal{T}\to\mathcal{T}_{int}=\exp[-N\gamma t+f(\sigma_1^z,\ldots,\sigma_N^z)t]$ and so

$$\langle S^j|\mathcal{T}_{int}(t)|S^i\rangle = \exp[-N\gamma t + f(S^i)t]\delta_{ij}. \tag{8}$$

For a given ensemble of initial configuration S^i our aim is to determine, which configurations S^j maximize the transition amplitude $Z_{ji}(t)$. From Eq. (6) we can already realize that the answer will depend only on the overlap between these two configurations and so the problem is reduced to finding the overlap m that maximizes Z_{ij}. Henceforth, we will refer to this maximum as $Z=\max_j Z_{ji}$, thus omitting, for the sake of simplicity, the dependence on the initial configuration index i. Of course, because of the large N limit we have $Z=\Sigma_j Z_{ji}$ as well.

The simplest fitness landscape for which the transition amplitudes Z_{ji} can be calculated exactly is the so-called single-peak (SP) fitness landscape. (The SP happens to be also the most studied fitness landscape in the quasispecies literature.) In this case, there is a single configuration—the master sequence S^0—with a high-fitness value NJ_0, whereas all other configurations have their fitness values set to zero. By choosing the master sequence as $S^0=(1,\ldots,1)$, the spin interactions for the SP landscape can be written as [23]

$$f_{SP}(\sigma_1^z,\ldots,\sigma_N^z) = NJ_0\left(\sum_k \sigma_k^z/N\right)^p \tag{9}$$

in the limit $p\to\infty$. What makes the SP problem analytically solvable was the remarkable finding that Z can be written in a factorized form

$$Z = \sum_j \int_0^t dt_1 \langle S^j|\mathcal{T}_{int}(t-t_1)|S^j\rangle\langle S^j|\mathcal{T}_{diff}(t_1)|S^i\rangle. \tag{10}$$

We refer the reader to the Appendix of Ref. [23]. for the detailed derivation of this result, which is based on the Trotter-Suzuki scheme [34] (see also [24,25]) that introduce infinitely many intermediate time steps between the initial and the final configurations. The key point for the factorization is the large p-spin interaction [see Eq. (9)] in the Hamiltonian, which results in a ground-state configuration with fitness much greater than the fitness of typical configurations. This is obvious for the SP landscape (except for the master, all configurations have zero fitness), but also holds for the REM landscape for which typical configurations have fitness on the order of $N^{1/2}$ whereas the ground state has fitness on order of N.

III. SP FITNESS LANDSCAPE

It is instructive to present the results for Z in the case of the single-peak landscape defined in the previous section and investigated in Ref. [23]. In particular, here we focus on the time dependence of the average overlap m between the configurations at time t and the initial configuration, a quantity which was not explored in that seminal work. First, we replace the sum over the final configurations S^j by an integral over all possible values of the overlap between the final and the initial configurations, taking into account that for large N there are $\rho(m)=\exp[Nh(m)]$ distinct configurations for a fixed overlap m, where

$$h(m) = -\frac{1+m}{2}\ln\frac{1+m}{2} - \frac{1-m}{2}\ln\frac{1-m}{2}. \tag{11}$$

Then we use Eqs. (6) and (8) to rewrite Z as

$$Z = \int_{-1}^{1} dm \int_0^t dt_1 \exp[NF_{SP}(m,t_1)], \tag{12}$$

where

$$F_{SP} = h(m) + \phi(m,t_1) - \gamma t + J_0(t-t_1). \tag{13}$$

The integrals over m and t_1 can be easily carried out for large N using Laplace's method as only the contribution of the maximum of F_{SP} is relevant for the evaluation of Z. We find a maximum at the extreme of the t_1 integration interval, i.e., $t_1=t$, which, according to Eq. (10), corresponds to a regime of pure diffusion in the sequence space. In fact, maximization of F_{SP} with respect to m for $t_1=t$ yields

$$m = \exp(-2\gamma t), \tag{14}$$

from where we obtain $F_{SP}=0$. Next, we consider the maximum within the integration intervals. The condition of maximum with respect to t_1 yields

$$(1+m)\tanh(\gamma t_1) + \frac{1-m}{\tanh(\gamma t_1)} - \frac{2J_0}{\gamma} = 0. \tag{15}$$

This is a quadratic equation for the unknown $\tanh(\gamma t_1)$, which has real solutions provided that $J_0\geq\gamma$ regardless of the value of the other unknown, m. This is an evidence that this solution describes the selective regime of the parallel selection-mutation evolution model. Now, maximization of F_{SP} with respect to m yields $m=\exp(-2\gamma t_1)$. The problem is that inserting this expression into Eq. (15) results in $J_0=\gamma$, and so for this particular situation m can take on any value, whereas t_1 is given by Eq. (15) and $F_{SP}=0$.

To understand what is happening here we recall that the average overlap between the sequences in the quasispecies distribution at equilibrium and the master sequence equals exactly 1 in the $N\to\infty$ limit. This is so despite the fact that the master sequences comprise only the fraction $1-\gamma/J_0$ of the total number of sequences at equilibrium. In the same vein, the overlap m between the initial configuration and the

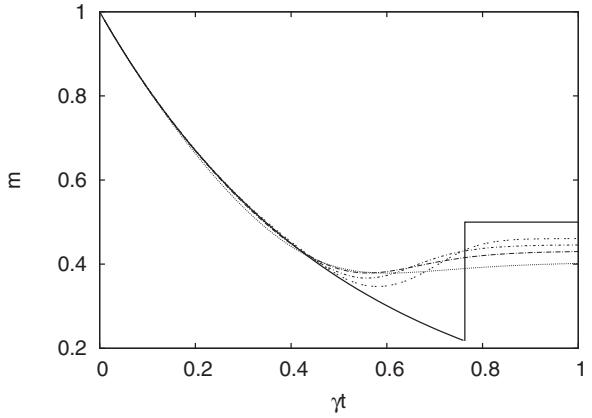

FIG. 1. Average overlap with the initial configuration as function of the scaled time γt for $J_0/\gamma=2$, $m_0=0.5$ and (broken lines from bottom to top at $\gamma t_{df}\approx 0.763$) $N=8$, 12, 16, and 24. The thick solid line is the theoretical prediction.

equilibrium configurations become identical to the overlap m_0 between the initial configuration and the master sequence, which is an arbitrary quantity defined by the initial conditions of the system. This explains the fact that the overlap m in Eq. (15) is not specified by the maximization conditions for $J_0=\gamma$: it is determined by the initial conditions, $m=m_0$.

To take into account the possibility that the dynamics reaches the close neighborhood of the master sequence, and so the overlap $m(t)$ freezes at the value m_0, in a finite time we now calculate the transition amplitude Z_{0i} between S^i and the master sequence S^0 in the time interval t, given that $m_0=\Sigma_k s_k^i s_k^0/N$. Since the final state is fixed the entropic term Eq. (11) must be dropped and we find

$$Z_{0i} \propto \exp\{N[\phi(m_0,t_1) - \gamma t + J_0(t-t_1)]\}, \tag{16}$$

where t_1 is given by Eq. (15) with $m=m_0$. Recalling that $F_{SP}=0$ for the diffusive regime Eq. (14), the selective regime takes over at time t such that $\phi(m_0,t_1)-\gamma t+J_0(t-t_1)>0$ [23]. Figure 1, which exhibits the time dependence of the overlap m, summarizes these results for a particular choice of J_0/γ and m_0. The jump of the overlap m at γt_{df} signals the transition between the diffusive and the selective (frozen) dynamic regimes. We note that for the value of $J_0/\gamma=2$ used in the figure, the overlap jumps up if $m_0>0.112$ and jumps down otherwise. The transition between the two regimes is continuous for $m_0\approx 0.122$. As illustrated in Fig. 1, the results of the numerical integration of the system of Eqs. (1) using the Runge-Kutta method show a clear trend to converge to the theoretical predictions as the sequence length N increases.

To conclude this brief overview of the parallel mutation-selection dynamics for the SP landscape we mention that the mean fitness R of the population is zero in the diffusive regime and $R=J_0-\gamma$ (i.e., J_0 times the frequency of master sequences in the population, $1-\gamma/J_0$) in the selective phase.

IV. REM FITNESS LANDSCAPE

In this case the fitness landscape is given by [13,14]

$$f(s_1,\ldots,s_N) = \sum_{i_1<i_2\ldots<i_p} J_{i_1\ldots i_p} s_{i_1}\ldots s_{i_p}, \tag{17}$$

where the couplings $J_{i_1\ldots i_p}$ are Gaussian distributed random variables of zero mean and variance $\langle J^2_{i_1\ldots i_p}\rangle = J^2 p!/(2N^{p-1})$. Taking the limit $p\to\infty$ in Eq. (17) results in 2^N independent energy levels, $E\equiv -f(s_1,\ldots,s_N)$, distributed by a Gaussian distribution

$$w(E) = \frac{1}{J\sqrt{\pi N}}\exp\left(-\frac{E^2}{NJ^2}\right). \tag{18}$$

The equilibrium statistical mechanics of the quantum Ising model in a transverse field, Eq. (4), with spin interactions given by Eq. (17) was studied in Ref. [24]. In the zero-temperature limit, which is the limit relevant to our analysis, there are two phases, namely, a spin-glass or frozen phase that occurs for large J, and a paramagnetic phase. The discontinuous transition between these phases takes place at $J/\gamma=1/\sqrt{\ln 2}\approx 1.201$ [24]. Clearly, within our evolutionary interpretation of the model, this phase transition corresponds to the error threshold phenomenon: for mutation rates greater than $J\sqrt{\ln 2}$ the adaptive information stored in the fitness landscape no longer affects the frequencies of sequences in the population, which become uniformly distributed.

Because of the presence of the quenched random variables $J_{i_1\ldots i_p}$, the derivation of the equations for the dynamics of the REM is more involved compared with that for the SP landscape. A rigorous derivation of the factorization Eq. (10) can be done using the Trotter-Suzuki scheme [24,25,34] as in the SP fitness landscape [23]. Here we give a qualitative derivation based on the general results described in Sec. II.

Effectively, we simply must replace $f(S^i)$ in Eq. (8) by E_i (i.e., by the energy of the initial configuration S^i), which amounts to replacing J_0 in Eq. (13) by E_i/N. Since our final results must be averaged over the energies of the final configurations S^j [see Eq. (10)] we have

$$Z = \int_0^t dt_1 \int_{-1}^{1} dm \int \frac{dE}{J\sqrt{\pi N}}\theta\left[h(m)-\left(\frac{E}{NJ}\right)^2\right] \times \exp\left[-\frac{E^2}{NJ^2}+E(t-t_1)\right] \times \exp[Nh(m)+N\phi(m,t_1)-N\gamma t]. \tag{19}$$

Here, the theta function enforces the constraint

$$h(m)-\left(\frac{E}{NJ}\right)^2 \geq 0, \tag{20}$$

which guarantees that the average number of configurations with energy E and overlap m with the initial configuration, given by $\exp(Nh(m)-E^2/NJ^2)$, is exponentially large, so that Z becomes a self-averaging quantity [13,16]. Hence Eq. (19) describes a typical situation of the dynamics at a fixed time t. Strictly, this equation is valid when the energy of the initial configuration E_i is larger then $-\gamma$. We will discuss later the corrections necessary to describe the case where this condition is violated. In addition, we assume that the overlap m_0

between the ground-state configuration and the initial configuration is zero.

The crucial step now is to evaluate the integral over E in Eq. (19) via Laplace's integration for fixed m and t_1. Noting that the result of the integration depends on whether the critical point $E^*=NJ^2(t-t_1)/2$ satisfies or not the constraint Eq. (20) and dropping trivial multiplicative factors, we rewrite Z as

$$Z_D = \int_0^t dt_1 \int_{-1}^{1} dm \exp[NF_D(m,t_1)], \tag{21}$$

where

$$F_D = h(m) + \phi(m,t_1) - \gamma t + J^2(t-t_1)^2/4 \tag{22}$$

provided that

$$h(m) - J^2(t-t_1)^2/4 > 0, \tag{23}$$

or

$$Z_{SG} = \int_0^t dt_1 \int_{-1}^{1} dm \exp[NF_{SG}(m,t_1)], \tag{24}$$

where

$$F_{SG} = \phi(m,t_1) - \gamma t + J\sqrt{h(m)}(t-t_1) \tag{25}$$

in the case that

$$h(m) - J^2(t-t_1)^2/4 < 0. \tag{26}$$

Equation (24) results when the critical point E^* is outside the energy integration interval, and so the argument of the exponential is maximized by the energy E at the extreme of that interval, namely, $E=NJ\sqrt{h(m)}$. As before, for large N we need to find the values of m and t_1 that maximize the arguments of the exponentials, Eqs. (22) and (25). The correct solution is then the one that corresponds to the largest of Z_D and Z_{SG}, i.e., $Z=\max\{Z_D,Z_{SG}\}$.

We begin with the analysis of Z_D, Eq. (21). Calculation of the extreme of $F_D(m,t_1)$ with respect to m and t_1 yields $m=\exp(-2\gamma t+4\gamma^2/J^2)$ and $t_1=t-2\gamma/J^2$, so that $F_D=-\gamma^2/J^2<0$. Next, we must evaluate F_D at the upper extreme of the t_1 integration interval, i.e., at $t_1=t$. This is the pure diffusion regime discussed in Sec. III which results in Eq. (14) and $F_D=0$. The lower extreme $t_1=0$ yields $F_D\to-\infty$ and the extremes of the m integration interval (i.e., $m=\pm 1$) need not be considered because $h(m=\pm 1)=0$ and so the condition Eq. (23) is violated. We note that the solution given by Eq. (14), which describes the pure drift or diffusion in the sequence space, exists for all parameter values since $h(m)\geq 0$ and so the inequality Eq. (23) is always satisfied. In addition, since solution [Eq. (14)] yields the largest value of the exponent F_D, the other solutions must be discarded.

We turn now to the analysis of Z_{SG}, Eq. (24). As before, we start by the maximization of $F_{SG}(m,t_1)$ with respect to both integration variables, m and t_1. At the maximum, we find that the values of these variables are given by the solution of the equations

$$\ln\tanh(\gamma t_1) + \frac{J}{2}\frac{(t-t_1)}{\sqrt{h(m)}}\ln\left(\frac{1+m}{1-m}\right) = 0 \tag{27}$$

and

$$(1+m)\tanh(\gamma t_1) + \frac{1-m}{\tanh(\gamma t_1)} - \frac{2J}{\gamma}\sqrt{h(m)} = 0. \tag{28}$$

These equations have to be solved numerically, but the solution is simple because Eq. (28) can be rewritten as a quadratic equation $y\equiv\tanh(\gamma t_1)<1$, which then can be written explicitly in terms of the unknown m. Regardless of the value of m, this quadratic equation has real solutions provided that $J/\gamma>1/\sqrt{\ln 2}$ and so we identify this dynamic regime with the frozen spin-glass phase of the quantum version of REM [24]. In addition, in the case that both roots of y are physical (i.e., less than 1), our numerical analysis indicates that we should always choose the smaller root since it corresponds to the largest value of the exponent F_{SG}.

To conclude the analysis of Z_{SG}, we must consider the contributions from the extremes of the integration intervals. The extreme $t_1=t$ is discarded because it violates condition Eq. (26), whereas the contribution of $t_1=0$ can be ignored because it yields $F_{SG}\to-\infty$. Regarding the extremes $m=\pm 1$, we find that in this case F_{SG} is maximum when t_1 takes on its extreme value, $t_1=t$. This corresponds to the contribution from the border $h(m)-J^2(t-t_1)^2/4=0$ which we will discuss in detail in the Appendix. Our numerical analysis indicates, however, that the border contribution can be ignored since it yields an exponent F_B [see Eq. (A2)] which is always smaller than the exponents obtained using the solution of the Eqs. (27) and (28).

In addition to the average overlap m between the initial and the configuration at time t, we can calculate the time dependence of the mean fitness R of the sequence population as well. The reasoning to derive R is sketched as follows. For the diffusive regime we have $R=0$ since the average fitness of any large sample of configurations visited in this regime is clearly zero for the REM fitness landscape. To estimate the mean fitness in the selective regime we just note the equivalence between the results for the single-peak landscape [see Eqs. (12) and (13)] and for the selective phase [see Eqs. (24) and (25)] if we identify J_0 with an effective, time-dependent single-peak fitness value $J_{eff}=J\sqrt{h(m)}$. (Note that for $t\to\infty$ we have $m\to 0$ so that $J_{eff}\to J\sqrt{\ln 2}$, which is the ground-state fitness value of the REM.) Since the population is formed by master copies with fitness value NJ_{eff} as well as by clouds of mutants with much smaller fitness (on the order of $N^{1/2}$) the mean fitness of the population in the selective regime becomes

$$R = J\sqrt{h(m)} - \gamma, \tag{29}$$

in accord with the well-known result for the (parallel) version of the single-peak landscape.

In summary, for fixed J/γ and γt we must solve the saddle-point Eqs. (27) and (28) to obtain the exponent F_{SG} (as well the saddle-point Eq. (A3) given in Appendix, but we have already mentioned that its contribution must be discarded) and then compare with the exponent of the diffusive

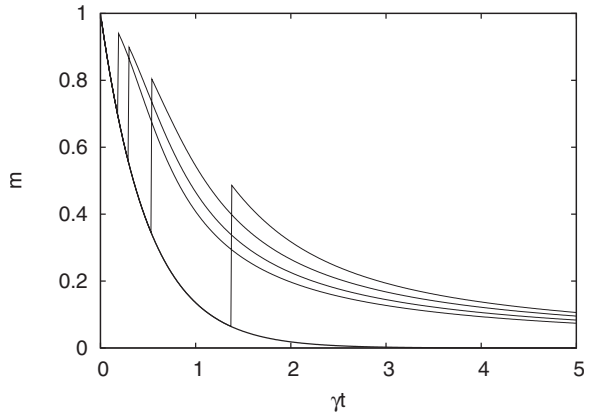

FIG. 2. Average overlap with the initial configuration as function of the scaled time γt for (thin solid lines from top to bottom at $\gamma t=2$) $J/\gamma=2$, 3, 4, and 5. The thick solid line is the function $\exp(-2\gamma t)$, which describes the overlap in the diffusive regime, $J/\gamma \leq 1/\sqrt{\ln 2}$.

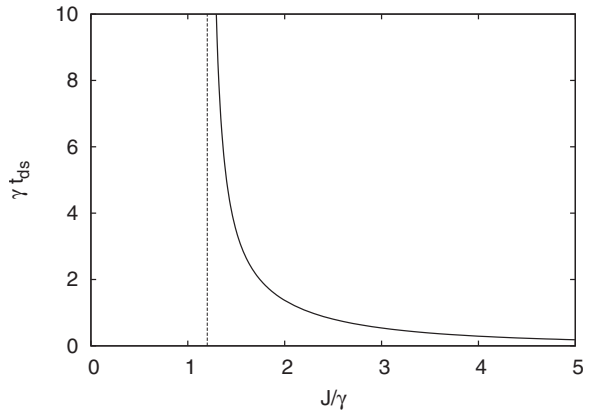

FIG. 3. Scaled critical time γt_{ds} at which the discontinuous dynamical transition between the diffusive and the selective regimes takes place as function of the dimensionless parameter J/γ. For $J/\gamma \leq 1/\sqrt{\ln 2}$ only the diffusive regime occurs. The selective regime is dominant in the region $t > t_{ds}$ (i.e., above the solid line).

regime $F_D=0$. If $F_{SG}>0$ we pick the value of m associated to the selective regime, otherwise we pick the diffusion solution given by Eq. (14).

A. Analysis of the results

Figure 2 illustrates the typical time evolution of the average overlap m with the initial configuration. We recall that the fitness of this initial configuration must be less than γ and its overlap with the ground-state configuration must be zero. As expected, for small γt the diffusive regime dominates and so m is given by Eq. (14). As γt increases further, the selective regime takes over rather abruptly, as shown by the discontinuity of the overlap m at a critical time value γt_{ds}. This bizarre behavior, which occurs also in the single-peak fitness landscape, is consequence of our characterization of the dynamics in a very large-dimensional sequence space by a single parameter: no such discontinuous behavior is observed when following the time evolution of the individual sequence frequencies, p_i for $i=1,\ldots,2^N$.

Since the properly scaled critical time γt_{ds} at which the discontinuity of the overlap m (and, consequently, of the mean fitness R) takes place can be used to separate the regions of validity of the two distinct dynamic regimes, in Fig. 3 we present the dynamic 'phase diagram' of the parallel evolutionary version of REM. As expected, γt_{ds} diverges as the J/γ approaches the value $1/\sqrt{\ln 2}$ which yields the equilibrium phase boundary between the paramagnetic and the frozen spin-glass phases. For large J/γ we find that γt_{ds} vanishes as $(J/\gamma)^{-2}$. Also of interest is the size of the overlap jump at γt_{ds}, shown in Fig. 4. The fact that this quantity exhibits a maximum could already be inferred from Fig. 2, since the overlap m tends to 1 or 0 in both dynamic regimes when J/γ approaches its extreme values.

B. Numerical integration

To complement our theoretical analysis, which is exact for infinite sequence lengths, we have carried the direct numerical integration of the linear system of ordinary Eqs. (2) for sequence lengths up to $N=24$ using the fourth-order Runge-Kutta integrator [39]. The stability of the numerical procedure benefited greatly from the fact the differential equations are linear. For $N \leq 10$ we can find all eigenvectors and eigenvalues of the symmetric matrix H and so solve the dynamics exactly for any t within an arbitrarily high numerical precision. Of course, the two numerical methods yield identical results provided that γt is not too large. Figures 5 and 6 summarize our numerical results for the $J/\gamma=4$. For each time t the data in these figures represent the average over 10^4 independent samples. The samples differ by the fitness values assigned to each configuration. For all samples the initial configuration was such as to have fitness value less than γ and zero overlap with the ground-state configuration.

Figure 5 is reassuring because the crossings of the lines for distinct N indicate the onset of a threshold phenomenon in the thermodynamic limit $N \to \infty$. In particular, to reproduce the analytical predictions, the first intersection point should tend to $\gamma t=0$ whereas the second should tend to

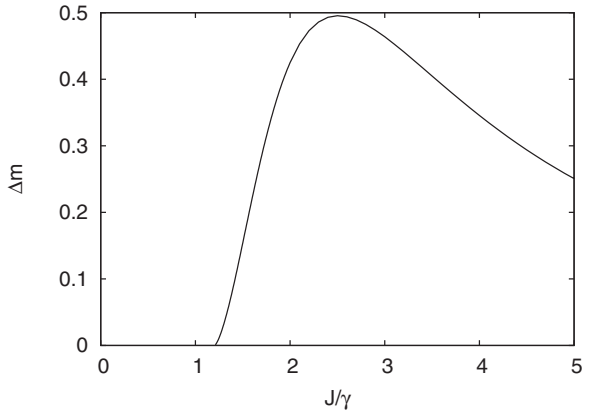

FIG. 4. Size of the overlap discontinuity Δm at $t=t_{ds}$ as function of the dimensionless parameter J/γ. The maximum of this curve occurs at $J/\gamma \approx 2.504$. For large J/γ we find that Δm vanishes as $(J/\gamma)^{-2}$.

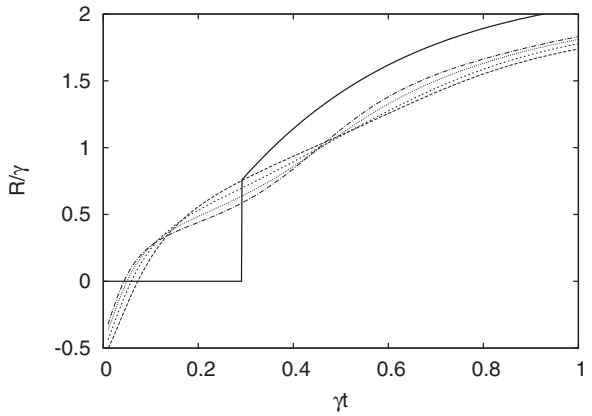

FIG. 5. Scaled mean fitness R/γ of the REM landscape as function of the scaled time γt for $J/\gamma=4$ and (broken lines from top to bottom at $\gamma t_{ds}\approx 0.292$) $N=12$, 16, 20, and 24. The thick solid line is the theoretical prediction.

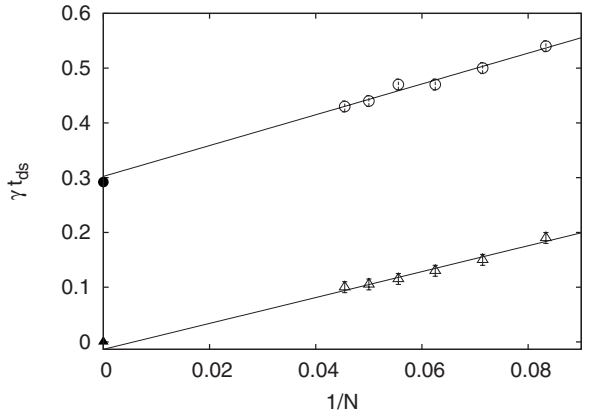

FIG. 7. Values of γt at which the mean fitnesses of sequences of length N and $N+2$ intersect shown as function of $1/N$ for $N=12$, 14, 16, 18, 20, and 22 for $J/\gamma=4$. The symbols △ and ○ identify the first and the second crossings, respectively (see Fig. 5), whereas the filled symbols indicate the theoretical predictions. The solid lines are the linear fittings used to obtain the extrapolated values at $1/N=0$.

$\gamma t_{ds}\approx 0.292$. To verify whether our data exhibit the correct trend, we show in Fig. 7 the values of γt at which the mean fitness curves intersect for successive values of N. The extrapolation to $N\to\infty$ yields $\gamma t=-0.01\pm 0.01$ for the first crossing and $\gamma t_{ds}=0.30\pm 0.01$ for the second crossing. The agreement with the theoretical prediction is excellent, given the short sequence lengths used in the numerical integration. Oddly enough, the dependence of the overlap m on the sequence length N, shown in Fig. 6, does not exhibit the characteristic crossings that signalize the onset of a threshold phenomenon in the thermodynamic limit, although the curve for $N=24$ already begins to take a shape that resembles the theoretical prediction. It seems that much larger sequence lengths are needed in order we can obtain clear evidence of a threshold phenomenon using the overlap data. We refer the reader to Ref. [40] for a full analysis of the finite size effects of the error threshold transition of the quasispecies model.

C. High-fitness initial configuration

To complete our analysis of the calculation of Z we consider now the situation in which the energy of the initial configuration E_i is such that $E_i<-\gamma$, i.e., this configuration has a relatively high fitness. In this case, we find a paramagnetic (but nondiffusive) regime where the system stays in the original configuration with a probability proportional to [see Eq. (8)]

$$Z=\exp[N(-E_i-\gamma)t] \tag{30}$$

and mean fitness $R=-E_i$. Since the argument of the exponential is always positive, this regime replaces the diffusive regime altogether. As t increases, it eventually becomes replaced by the selective regime at some threshold time $t'_{ds}>t_{ds}$. However, the dependence of t'_{ds} on the particular value E_i makes this case rather unattractive, as compared with the case where the initial configuration has a low-fitness value.

Finally, we note that the probability that $E_i<-\gamma$ is $\frac{1}{2}\mathrm{erfc}(\gamma/J\sqrt{N})$, which tends to 1/2 for large N, hence, we could more simply distinguish the two situations–high- and low-initial fitness–by verifying whether the energy of the initial configuration is positive or negative. More importantly, these two cases are equally likely and our penchant for the low-fitness initial configuration here is justified only by the generality of the results obtained in that case.

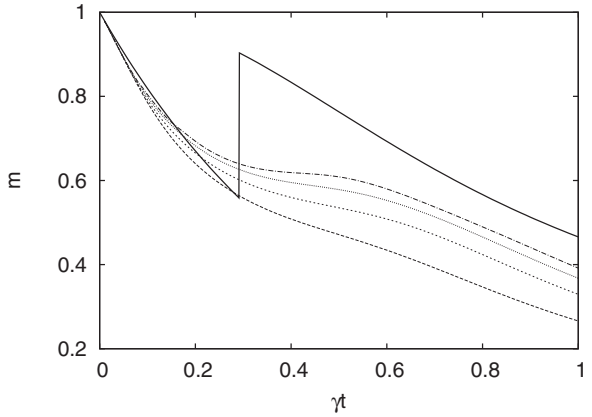

FIG. 6. Average overlap with the initial configuration as function of the scaled time γt for $J/\gamma=4$ and (broken lines from bottom to top at $\gamma t_{ds}\approx 0.292$) $N=12$, 16, 20, and 24. The thick solid line is the theoretical prediction.

D. Relaxation to equilibrium

The approach to the equilibrium state as $\gamma t\to\infty$ is particularly interesting because it is related to the speed of evolution, i.e., how long it takes for a random sequence to reach the global maximum of a rugged fitness landscape. In contrast with the finite-time dynamics described before, the results of the asymptotic analysis do not depend on the specific value of the fitness of the initial configuration. We still require, however, that the initial configuration has zero overlap with the ground state.

As we focus on the limit of large γt, the relevant equations to describe the system dynamics are Eqs. (27) and (28). From Fig. 2 we can see that $m\to 0$ in this limit and so Eq. (28) yields

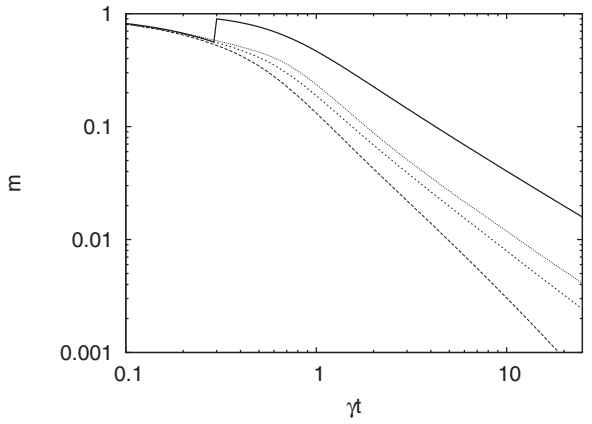

FIG. 8. Asymptotic dependence of the average overlap on γt for $J/\gamma=4$ and (broken lines from bottom to top) $N=6$, 8, and 10. The thick solid line is the theoretical prediction, which yields $m \propto 1/(\gamma t)$ [see Eq. (32)].

$$y = \kappa - \sqrt{\kappa^2 - 1}, \tag{31}$$

where $y=\tanh(\gamma t_1)$ and $\kappa=J\sqrt{\ln 2}/\gamma$. Since $y<1$ for $\kappa>1$, t_1 is finite and then, taking the limit $t\to\infty$ in Eq. (27), we find

$$m = \left(-\frac{\ln 2 \ln y}{\kappa}\right)\frac{1}{\gamma t}. \tag{32}$$

This important result indicates that relaxation to equilibrium, which is characterized by the ground-state configuration together with a cloud of very close mutant configurations (the quasispecies distribution) is given by a power law with exponent -1.

An estimate of the speed of evolution can be obtained by considering the prefactor of $1/\gamma t$ in Eq. (32). We find that this prefactor vanishes at the extremes $\kappa=1$ and $\kappa\to\infty$, and reaches a maximum at $\kappa\approx 1.810$ or $J/\gamma\approx 2.174$. (If we had included the curve for, say, $J/\gamma=1.5$ in Fig. 2 we could have observed this nonmonotonic behavior there.) This parameter setting corresponds then to the slowest convergence to equilibrium, i.e., the minimum speed of evolution. The maximum speed is obtained by setting $\kappa\to\infty$ (or $J/\gamma\to\infty$), which amounts to taking a vanishingly small mutation rate.

To check whether a similar power-law scaling for large times holds also for (infinite) populations of finite length sequences, we solved the linear system Eq. (2) through the direct diagonalization of H, which is feasible only for relatively small sequence lengths. Figure 8 summarizes our numerical results, which represent the average over 10^4 independent samples. We find that the finite N data is very well fitted by the scaling law $m\propto(\gamma t)^{-\alpha_N}$ with $\alpha_6=1.77$, $\alpha_8=1.36$, and $\alpha_{10}=1.17$. Assuming that $\alpha_\infty=1$ we find that these exponents, in turn, are described perfectly by the function $\alpha_N=1+7.48\exp(-0.38N)$, which indicates a very rapid approach to the value of the infinite-length exponent.

V. FERROMAGNETIC REM LANDSCAPE

In the ferromagnetic REM [13,27], we choose a particular configuration, say $S^0=(1,\ldots,1)$, and set its fitness value to J_0N. The other 2^N-1 configurations are assigned random fitness values $-E$ with E distributed by the Gaussian distribution Eq. (18). From the evolutionary modeling perspective, the fitness level produces a gap in the fitness landscape, which, as we show here, results in nontrivial dynamic consequences.

The quantum spin version of the ferromagnetic REM is defined by Hamiltonian Eq. (4) with the fitness function

$$f(s_1,\ldots,s_N) = \sum_{i_1<i_2\ldots<i_p} J_{i_1\ldots i_p} s_{i_1}\ldots s_{i_p} + NJ_0\left(\frac{1}{N}\sum_k s_k\right)^p, \tag{33}$$

where the multispin couplings $J_{i_1\ldots i_p}$ are defined as in Sec. IV. This fitness landscape is thus a linear combination of the SP and REM landscapes. The equilibrium statistical mechanics of the quantum ferromagnetic REM was studied in Ref. [25], where the condition for the existence of the ferromagnetic phase at zero temperature (i.e., for S^0 be the ground-state configuration) was found to be $J_0>J\sqrt{\ln 2}$. Here, we will consider only parameter settings that satisfy this condition.

As in the previous cases, we use the decomposition of the transition amplitude Z, Eq. (10), to solve the dynamics for the overlap m between the initial and the typical configurations at time t. The important change is that now the sum over the final configurations S^j in Eq. (10) does not include the master sequence S^0, which must be considered separately. Hence, we find that Z is given by a sum of two terms, the first is the REM contribution, Eq. (19), and the second is the SP contribution, Eq. (16). In particular, we focus on the case $m_0=0$ only, so that the latter equation becomes

$$Z_F = \exp\left\{N\left[\frac{1}{2}\ln\frac{\sinh(2\gamma t_1')}{2} - \gamma t + J_0(t-t_1')\right]\right\}, \tag{34}$$

where $y'\equiv\tanh(\gamma t_1')$ is given by the quadratic equation $(y')^2-2J_0y'/\gamma+1=0$ (see Eq. (15) with $m=m_0=0$), which has real solutions for $J_0\geq\gamma$. As the interesting situation is one where the spin-glass solution, given by Eqs. (27) and (28), exists as well, so that $J/\gamma>1/\sqrt{\ln 2}$, we have

$$\frac{J_0}{\gamma} > \frac{J}{\gamma}\sqrt{\ln 2} > 1, \tag{35}$$

so the existence of the ferromagnetic and spin-glass phases guarantees that y' is real.

To obtain the time evolution of $m(t)$ we first calculate $\ln Z_{SG}$ using Eq. (24) and $\ln Z_F$ using Eq. (34) for fixed t. (We take logarithms here because the relevant quantities are the expressions in the arguments of the exponentials that define the transition amplitudes.) If these two quantities are negative, we choose the diffusive solution, Eq. (14). If $\ln Z_F>\ln Z_{SG}$ then the system is in the ferromagnetic regime and so $m=0$; otherwise we choose m given by the spin-glass solution, Eqs. (27) and (28).

As the setting $J_0>J\sqrt{\ln 2}$ implies that the equilibrium phase is the ferromagnetic one, one must have $m=0$ for large γt. On the other hand, if the fitness of the initial configuration is not greater than γ (which we tacitly assume in this

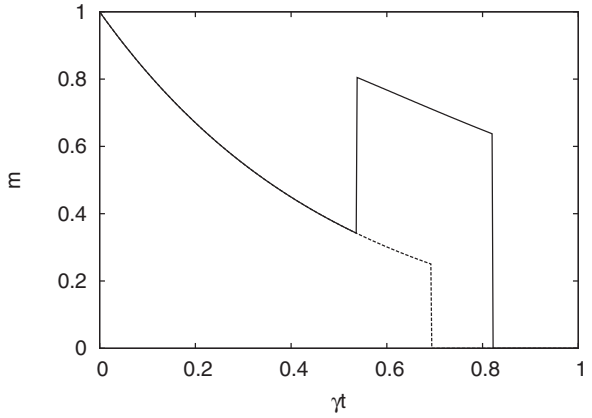

FIG. 9. Average overlap m as function of scaled time γt. The solid curve for $J_0/\gamma=J/\gamma=3$ shows a transition between the diffusive and the spin-glass regimes at $\gamma t=0.538$, and a transition between the spin-glass and the ferromagnetic regimes at $\gamma t=0.820$. The broken curve for $J_0/\gamma=3$ and $J/\gamma=2$ shows a situation where there is a direct transition between the diffusive and ferromagnetic regimes at $\gamma t=0.693$.

section), the diffusive regime dominates for small γt. The question is then whether an intermediate, spin-glass regime appears between these extremes. The answer is given in Fig. 9, which indicates that the appearance of the intermediate regime depends on the values of the parameters J and J_0. To determine the region in the space of parameters $(J/\gamma, J_0/\gamma)$ where the spin-glass regime interfaces the other two regimes, we have to calculate the value of J_0/γ such that the time t_{ds} at which the transition from the diffusive to the spin-glass regime coincides with the time t_{df} at which the diffusive regime transitions to the ferromagnetic one. Note that t_{ds} depends only on J as shown in Fig. 4. As for the time $t=t_{df}$ at which the transition between the diffusive and the ferromagnetic regimes takes place, it can be calculated analytically by setting $\ln Z_F=0$ (see [23]). The final result is

$$\gamma t_{df} = \frac{1}{4(\kappa_0 - 1)} \left\{ \kappa_0 \ln \frac{\kappa_0 + 1}{\kappa_0 - 1} + \ln[4(\kappa_0^2 - 1)] \right\}, \quad (36)$$

where $\kappa_0=J_0/\gamma$. The procedure for searching the values of J_0/γ, for fixed J/γ, at which $t_{ds}=t_{df}$ is implemented numerically and the result is shown in Fig. 10. Above the thick solid line there are only two dynamic regimes, the diffusive and the ferromagnetic, and the time t_{df} at which the transition occurs is given by Eq. (36). In what follows we will concentrate on the study of the dynamics for the parameters in the region below that line, where the three dynamic regimes are present. In particular, we will focus on the transition between the spin glass and the ferromagnetic regimes, which happens at time $t=t_{sf}$.

Before we offer an analytical approximation to t_{sf}, it is instructive to study numerically its dependence on J_0/γ and J/γ. This is shown in Fig. 11, from where it becomes clear that t_{sf} is defined in a narrow region of the parameter space, determined by the conditions that the ferromagnetic phase exists and that the spin-glass regime interfaces the diffusive and ferromagnetic regimes. Figure 12 shows the discontinuity of the overlap at t_{sf}. Since the overlap in the ferromagnetic regime is zero, the jump Δm is actually the overlap in the spin-glass phase.

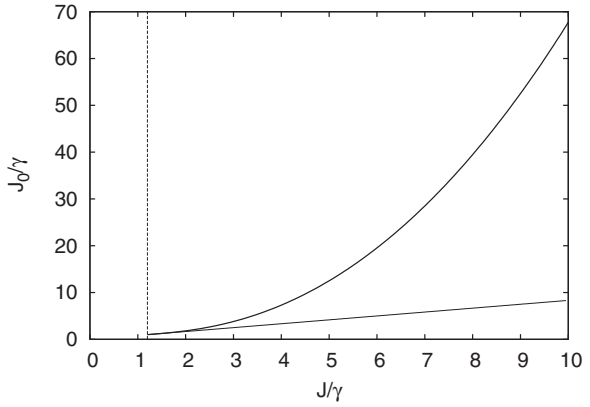

FIG. 10. The spin-glass regime interfaces the diffusive and the ferromagnetic regimes only in the region of parameters located below the thick solid curve. This curve begins at the point $(1/\sqrt{\ln 2}, 1)$ and diverges as J^2 for large J. The thin solid straight line is $J_0=J\sqrt{\ln 2}$, below which the ferromagnetic phase is absent.

The divergence of t_{sf} and the vanishing of $\Delta m=m$ as J_0 approaches $J\sqrt{\ln 2}$ allows us to derive an analytical expression for t_{sf} in this limit. In fact, Eq. (32) already provides an explicit expression for m, namely,

$$m = -\frac{\sqrt{\ln 2}\,\ln y}{J t_{sf}}, \quad (37)$$

since t_{sf} is large. The equation that defines t_{sf} is obtained by equating $\ln Z_F/N$ to F_{SG},

$$\ln\left[\frac{\sinh(2\gamma t_1')}{\sinh(2\gamma t_1)}\right] + m \ln \tanh(\gamma t_1) + 2J\sqrt{h(m)}t_1 = +2J_0 t_1' - 2[J_0 - J\sqrt{h(m)}]t_{sf}. \quad (38)$$

Recalling that for $\epsilon \equiv (J_0 - J\sqrt{\ln 2})/J_0 \to 0$ we have $\kappa \to \kappa_0$ and so $t_1' \to t_1$, we rewrite this expression as

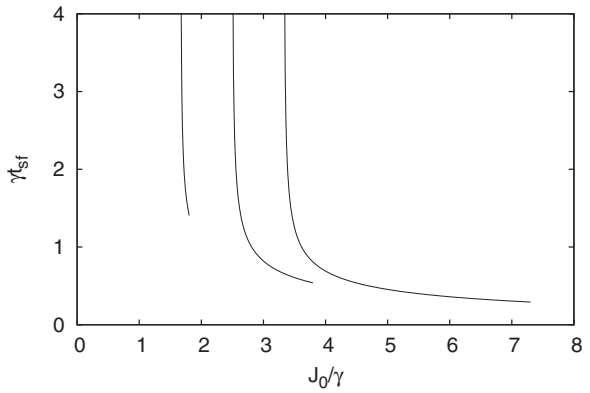

FIG. 11. Scaled time at which the spin-glass transitions to the ferromagnetic for (left to right) $J/\gamma=2$, 3, and 4. This transition occurs only within a limited region of the parameter space, as illustrated in Fig. 10. The divergences occur at $J_0=J\sqrt{\ln 2}$.

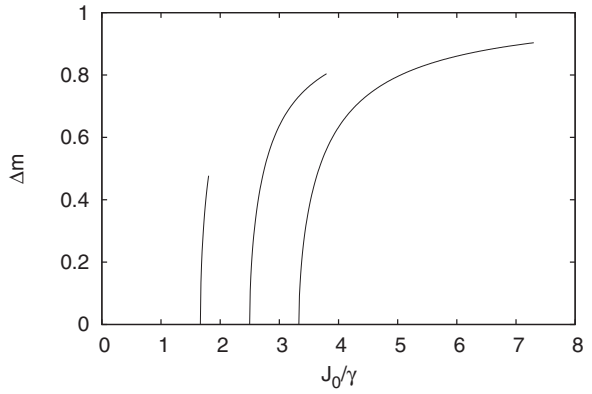

FIG. 12. The overlap discontinuity Δm at $t=t_{sf}$ for (left to right) $J/\gamma=2$, 3 and 4. Since the overlap is zero in the ferromagnetic regime, Δm equal the overlap in the spin-glass regime.

$$t_{sf} = -m\frac{\ln \tanh(\gamma t_1)}{2J_0\epsilon}, \tag{39}$$

where we used $h(m)\to \ln 2$ for $m\to 0$. Finally, inserting m from Eq. (37) into this expression yields

$$\gamma t_{sf} = -\left(\frac{\ln 2}{2\epsilon}\right)^{1/2}\frac{1}{\kappa_0}\ln(\kappa_0 - \sqrt{\kappa_0^2 - 1}). \tag{40}$$

As $m\sim 1/(\gamma t_{sf})$ we find the typical mean-field result $m \sim \epsilon^{1/2}$ at the transition.

Since t_{sf} (or t_{df}, depending on the parameter settings) is the waiting time for evolution to lead the system close to its optimal fitness situation, it is interesting to see whether this waiting time can be minimized by a proper choice of parameters (the mutation rate, for example). For fixed κ_0, we note that t_{sf} must satisfy the constraint $t_{sf} > t_{df}$ in the case the spin-glass regime is present. Hence, the minimum waiting time $t_{\min}$ is obtained by equating the waiting times given in Eqs. (36) and (40). Of course, since $\epsilon\to 0$ we must set $\kappa_0 \to 1$ in the former equation. Keeping leading order terms in $\delta=\kappa_0-1$, Eq. (36) becomes $\gamma t_{df}\sim(\ln 2)/\delta$, whereas Eq. (40) reduces to $\gamma t_{sf}\sim(\delta \ln 2/\epsilon)^{1/2}$. Equating these results yields $\delta=(\epsilon \ln 2)^{1/3}$ so that the minimum time to reach the optimal fitness situation is

$$\gamma t_{\min} = \frac{(\ln 2)^{2/3}}{\epsilon^{1/3}}. \tag{41}$$

This expression is valid only in the limits $J_0/\gamma\to 1$ and $J/\gamma\to 1/\sqrt{\ln 2}$.

VI. CONCLUSION

Most of the techniques from statistical mechanics employed in the study of evolutionary models, such as Eigen's quasispecies model, are manageable only in the stationary regime $t\to\infty$ (see, e.g., [12,15,22,41]). Although the equilibrium analysis provides valuable insights into the behavior of these models, a complete study of the dynamics is indispensable as evolution is all about species dynamics, after all.

In this contribution, we present an exact solution for the evolutionary dynamics in an extremely rugged fitness landscape, Derrida's REM [13]. The evolutionary model studied is the quasispecies model with a parallel mutation-selection scheme, in which mutations are decoupled from replication [36]. This scheme can be mapped in Ising quantum chain in a transverse field [22], and the dynamics can be solved using the Suzuki-Trotter formalism as done in the case of the SP landscape [23]. In fact, the similarity between the SP and REM-like fitness landscapes regarding their steady-state distributions—they are identical within the accuracy $\sim 1/\sqrt{N}$—is well known [16], and here we explore it to derive the evolutionary dynamics on the REM landscape using the SP landscape results.

The (infinite) population is initially homogeneous, i.e., all sequences are identical to a reference sequence chosen such that its overlap with the highest-fitness sequence is zero. In addition, most of our results are based on the assumption that the fitness of this reference sequence is negative. We note that in the parallel mutation-selection scheme, we have a Malthusian fitness which basically measures the difference between the reproduction and death rates, and so can take on positive and negative values as well.

At each time t, the population is characterized by the average overlap with the reference sequence $m(t)$ as well as by the mean fitness $R(t)$. As expected, in the case the initial configuration has low fitness (i.e., the fitness value is less than the mutation rate per site γ), the dynamics for small t corresponds to a random drift in the sequence space with m decreasing exponentially with increasing t [see Eq. (14)]. Selection, which encodes information in the fitness landscape, has no role in the diffusive regime. We find, quite remarkably, that m undergoes a discontinuous transition at some finite $t=t_{ds}$ (see Fig. 2) when the dynamics enters a spin-glass regime in which m vanishes as $1/t$ for large t. As opposed to the SP landscape (and to the ferromagnetic version of REM; see below), the dynamics needs an infinite time to reach the regions close to optimal fitness sequence. When the initial configuration already has high fitness (i.e., the fitness value is greater than γ) the diffusive regime is replaced by a pattern of stasis: the dynamics freezes at the initial configuration (i.e., $m=1$ and $R=-E_i$) for a certain length of time $t_i > t_{ds}$ where $t_i=t_i(E_i)$ and then undergoes a discontinuous transition to the spin-glass regime.

In addition to the REM fitness landscape, we considered also the somewhat more realistic ferromagnetic-REM landscape which, as it is clear from Eq. (33), can be viewed as a simple combination of the REM and SP fitness landscapes. For some parameter settings (see Fig. 9), we find three distinct dynamic regimes: the diffusive, spin-glass and the ferromagnetic regimes. The transitions between these regimes are signaled by discontinuities of the overlap as well as of the mean fitness. In a parameter setting such that the equilibrium phase is the ferromagnetic one, the time to reach the optimal sequence is finite, as in the SP case, but diverges near the (equilibrium) transition points. As in the case of the ordinary REM, the diffusive regime is replaced by stasis when the initial configuration has a high-fitness value.

The discontinuous transitions between the different dynamic regimes are similar to the punctuations, during which evolution proceeds very rapidly, observed in finite population simulations [7,8]. In fact, one of the first theoretical models

to reproduce the punctuated equilibrium phenomenon made explicit use of the effect of random genetic drift, which results from the finitude of the population, to promote the transition between alternative fitness peaks [42]. Since our results were derived within the infinite-population assumption, this process cannot be responsible for the observed punctuations. Alternatively, punctuations are predicted by models in which initially low frequency beneficial mutation becomes dominant in a few generations after a certain frequency threshold is overcome [43,44]. This is the process responsible for the punctuations observed in our model as well as in microbial population experiments [9].

The infinite size population assumption behind the quasispecies-like evolution model considered here is a theoretical approximation only, and finite population size effects are undoubtedly important. The discrete-time evolutionary dynamics on a REM-like fitness landscape has been extensively investigated in the literature for the finite population case [18–21,45]. Analytical approximations and numerical simulations have yielded many interesting results about record statistics and crossover transitions. We note, however, that the exact solution of the deterministic model exhibits a much richer dynamical structure. It would be interesting to see whether there are any vestiges of the discontinuous transitions in the case of finite but large populations and, in particular, how the coalescent time statistics are affected by these regime changes [45].

While our main interest is the investigation of the evolutionary dynamics, our results bear on information theory as well [46], as they can be viewed as the exact analytical solution for the decoding process (relaxation to the ferromagnetic configuration) of optimal codes [27–31]. In particular, we conjecture that Eq. (41) is universal for some classes of dynamics near the error threshold-like transitions. In fact, the connection of evolution models with information theory was first pointed out by Eigen, who actually used information theoretical arguments to derive an expression for the error threshold in the SP landscapes [10]. More recently, the relation between molecular biology and information theory was discussed in Refs. [47,48].

In general, almost any fitness landscape can be qualitatively identified with one of three classes: ferromagnetic, spin-glass and ferromagnetic spin-glass like. The first class, which exhibits a finite relaxation time to the optimum, seems too simplistic to bear on real biological situations. The spin-glass fitness landscape, on the other hand, exhibits an infinite relaxation time to the optimum, which then could never be reached by the evolutionary dynamics. The third class, which combines the complexity of the spin-glass landscape with a finite relaxation time, seems to be the preferable one from the evolutionary perspective. Thus natural selection seems to choose the type of fitness landscape that works more efficiently as an information processing system.

The picture that emerges from computer experiments with digital organisms [49] resembles the case of SG fitness case. Although this random macroevolution scenario may be described by a spin-glass fitness landscape, Nature's preference seems to be for the ferromagnetic spin-glass landscape, as manifested, for example, by protein evolution. In fact, it is known that proteins differ substantially from random heteropolymers, and that random heteropolymers can be described by the ordinary REM, whereas biological polymers are described quite well by the ferromagnetic REM [50,51]. Hence, the genome, which codes the information to assemble the proteins, reveals ferromagnetic or ferromagnetic spin-glass like fitness landscape. This is close to the idea of channels in evolution [52]. During the evolution, there are large rearrangements of the genome, in addition to the point substitutions considered here. This large transpositions resemble the multiscale optimization in computer science: perhaps Nature takes advantage of large gene rearrangements, whenever the search for optimum by means of simple substitutions becomes too slow [53]. These large events, as well as the simultaneous point mutations in two or three adjacent sites, are permitted because they practically do not affect the error threshold, while the evolution dynamics changes drastically, e.g., a relaxation time of about 10^6 years in the case of single point mutations is reduced to 100 years when triplet adjacent mutations are allowed [53]. We note that simultaneous mutations in two or three random sites yield the same slow relaxation as in the case of a single point substitution.

In the theory of computation, optimization problems are classified as polynomially solvable if the relaxation time to the optimum scales with some power of the problem size, and as NP-complete or as NP-hard otherwise, i.e., when the relaxation time scales exponentially with the problem size [54]. Hence, the channel-like evolution schemes are not only ferromagnetic-type fitness, but also resemble the fast computational schemes of polynomial class.

ACKNOWLEDGMENTS

The work at Yerevan was supported in part by the VolkswagenStiftung through a "Quantum Thermodynamics" grant. The research at São Carlos was supported in part by CNPq and FAPESP, Project No. 04/06156-3. D.B.S. acknowledges the hospitality of the Instituto de Física de São Carlos, Universidade de São Paulo, and acknowledges FAPESP travel Grant No. 08/10420-9 for support of his visit to São Carlos.

APPENDIX: BORDER CONTRIBUTION TO Z

To complete the analysis of the integrals in Eqs. (21) and (24) for large N, we must consider the contribution from the border $h(m)=J^2(t-t_1)^2/4$. Clearly, in this case we have $Z_D=Z_{SG}=Z_B$ with

$$Z_B = \int_{-1}^{1} dm \, \exp[NF_B(m)], \tag{A1}$$

where

$$F_B = 2h(m) + \phi(m,t_1) - \gamma t \tag{A2}$$

and $t_1=t_1(m)$ is a function of m given by the border equation. Maximization of F_B with respect to m yields the saddle-point equation

$$\ln\left(\frac{1+m}{1-m}\right)+\frac{1}{2}\ln\tanh(\gamma t_1) = \frac{\gamma\ln\left(\frac{1+m}{1-m}\right)}{4J\sqrt{h(m)}}\left[(1+m)\tanh(\gamma t_1)+\frac{1-m}{\tanh(\gamma t_1)}\right], \tag{A3}$$

which must be solved numerically. At the extremes $m=\pm 1$ we have $t_1=t$ and so $F_B=\ln[1\pm\exp(-2\gamma t)]-\ln 2\leq 0$. Our extensive numerical analysis comparing the three exponents $F_D=0$, F_{SG} and F_B indicates that whenever $F_B>0$ we have $F_{SG}>F_B$ and so the contribution from the border can be neglected in comparison with those from the inner saddle points discussed in the main text.

[1] S. Kauffman and S. Levin, J. Theor. Biol. **128**, 11 (1987).
[2] P. Schuster and P. F. Stadler, Complexity **8**, 34 (2002).
[3] M. Mezard, G. Parisi, and M. A. Virasoro, *Spin Glass Theory and Beyond* (World Scientific, Singapore, 1987).
[4] D. L. Stein and P. W. Anderson, Proc. Natl. Acad. Sci. U.S.A. **81**, 1751 (1984).
[5] A. S. Perelson and C. A. Macken, Proc. Natl. Acad. Sci. U.S.A. **92**, 9657 (1995).
[6] H. Flyvbjerg and B. Lautrup, Phys. Rev. A **46**, 6714 (1992).
[7] P. Sibani, M. R. Schmidt, and P. Alstrom, Phys. Rev. Lett. **75**, 2055 (1995).
[8] I. Aranson, L. S. Tsimring, and V. Vinokur, Phys. Rev. Lett. **79**, 3298 (1997).
[9] S. F. Elena, V. S. Cooper, and R. E. Lenski, Science **272**, 1802 (1996).
[10] M. Eigen, Naturwiss. **58**, 465 (1971).
[11] I. Leuthäusser, J. Stat. Phys. **48**, 343 (1987).
[12] P. Tarazona, Phys. Rev. A **45**, 6038 (1992).
[13] B. Derrida, Phys. Rev. Lett. **45**, 79 (1980); Phys. Rev. B **24**, 2613 (1981).
[14] D. J. Gross and M. Mézard, Nucl. Phys. B **240**, 431 (1984).
[15] S. Franz, L. Peliti, and M. Sellitto, J. Phys. A **26**, L1195 (1993).
[16] S. Franz and L. Peliti, J. Phys. A **30**, 4481 (1997).
[17] H. A. Orr, Genetics **163**, 1519 (2003).
[18] J. Krug and C. Karl, Physica A **318**, 137 (2003).
[19] K. Jain and J. Krug, J. Stat. Mech.: Theory Exp. (2005) P04008.
[20] C. Sire, S. Majumdar, and D. S. Dean, J. Stat. Mech.: Theory Exp. (2006) L07001.
[21] K. Jain, Phys. Rev. E **76**, 031922 (2007).
[22] E. Baake, M. Baake, and H. Wagner, Phys. Rev. Lett. **78**, 559 (1997).
[23] D. B. Saakian and C.-K. Hu, Phys. Rev. E **69**, 046121 (2004).
[24] Y. Y. Goldschmidt, Phys. Rev. B **41**, 4858 (1990).
[25] D. B. Saakyan, Theor. Math. Phys. **94**, 123 (1993).
[26] D. B. Saakian, O. Rozanova, and A. Akmetzhanov, Phys. Rev. E **78**, 041908 (2008).
[27] N. Sourlas, Nature (London) **339**, 693 (1989).
[28] D. B. Saakian, JETP Lett. **55**, 198 (1992); A. E. Allakhverdyan and D. B. Saakian, Nucl. Phys. B **498**, 604 (1997).
[29] Y. Kabashima and D. Saad, J. Phys. A **37**, R1 (2004).
[30] H. Nishimori, Prog. Theor. Phys. **66**, 1169 (1981).
[31] P. Rujan, Phys. Rev. Lett. **70**, 2968 (1993).
[32] D. B. Saakian, Phys. Rev. E **71**, 016126 (2005).
[33] J. J. Hopfield, Proc. Natl. Acad. Sci. U.S.A. **79**, 2554 (1982).
[34] M. Suzuki, Prog. Theor. Phys. **56**, 1454 (1976).
[35] J. F. Crow and M. Kimura, *An Introduction to Population Genetics Theory* (Harper & Row, New York, 1970).
[36] T. Wiehe, E. Baake, and P. Schuster, J. Theor. Biol. **177**, 1 (1995).
[37] J. Hofbauer and K. Sigmund, *The Theory of Evolution and Dynamical Systems* (Cambridge University Press, Cambridge, UK, 1988).
[38] C. J. Thompson and J. L. McBride, Math. Biosci. **21**, 127 (1974); B. L. Jones, R. H. Enns, and S. Rangnekar, Bull. Math. Biol. **38**, 15 (1976).
[39] W. H. Press, S. A. Teukolsky, W. T. Vetterling, and B. P. Flannery, *Numerical Recipes in Fortran 77* (Cambridge University Press, Cambridge, UK, 1992).
[40] P. R. A. Campos and J. F. Fontanari, Phys. Rev. E **58**, 2664 (1998).
[41] S. Galluccio, Phys. Rev. E **56**, 4526 (1997).
[42] C. M. Newman, J. E. Cohen, and C. Kipnis, Nature (London) **315**, 400 (1985).
[43] R. E. Lenski, M. R. Rose, S. C. Simpson, and S. C. Tadler, Am. Nat. **138**, 1315 (1991).
[44] P. A. Johnson, R. E. Lenski, and F. C. Hoppensteadt, Proc. R. Soc. London, Ser. B **259**, 1 (1991).
[45] C. O. Wilke, P. R. A. Campos, and J. F. Fontanari, J. Exp. Zool. **294**, 274 (2002).
[46] I. Chisarand and J. Korner, *Information Theory* (Mir, Moscow, 1985).
[47] C. Adami, C. Ofria, and T. C. Collier, Proc. Natl. Acad. Sci. U.S.A. **97**, 4463 (2000).
[48] C. Adami, Phys. Life Rev. **1**, 3 (2004).
[49] G. Yedid and G. Bell, Nature (London) **420**, 810 (2002).
[50] J. D. Bryngelson and P. G. Wolynes, Proc. Natl. Acad. Sci. U.S.A. **84**, 7524 (1987).
[51] V. S. Pande, A. Yu. Grossberg, and T. Tanaka, Rev. Mod. Phys. **72**, 259 (2000).
[52] C. H. Waddington, Nature (London) **150**, 563 (1942).
[53] E. V. Nimwegen and J. P. Crutchfield, Bull. Math. Biol. **62**, 799 (2000).
[54] C. Papadimitrow, *Computational Complexity* (Addison-Wesley, Reading, 1994).